



Cobalt and Iron Complexes with N-heterocyclic Ligands as Pyrolysis Precursors for Oxygen Reduction Catalysts



Federico Roncaroli^{a,b,*}, Emiliano S. Dal Molin^a, Federico A. Viva^a, Mariano M. Bruno^{a,c}, Emilia B. Halac^{a,c}

^a Departamento de Física de la Materia Condensada, Centro Atómico Constituyentes, Comisión Nacional de Energía Atómica (CNEA), Avenida General Paz 1499, (1650) San Martín, Buenos Aires, Argentina

^b Departamento de Química Inorgánica, Analítica y Química Física, Facultad de Ciencias Exactas y Naturales, Universidad de Buenos Aires, Ciudad Universitaria, Pabellón II, (1428) Buenos Aires, Argentina

^c Escuela de Ciencia y Tecnología, Universidad Nacional de General San Martín, Martín de Irigoyen 3100, (1650) San Martín, Buenos Aires, Argentina

ARTICLE INFO

Article history:

Received 19 February 2015

Received in revised form 21 May 2015

Accepted 22 May 2015

Available online 27 May 2015

Keywords:

polymer electrolyte membrane

fuel cell

non-noble catalyst

ORR

Platinum-free

ABSTRACT

Cobalt and Iron based catalysts for the Oxygen Reduction Reaction (ORR) are a promising alternative to the use of Pt in Polymer Electrolyte Fuel Cells (PEMFC). A systematic study on the influence of the nitrogenated ligand in the precursor complex on the ORR activity was performed. Several Fe and Co complexes were prepared with different N-heterocyclic ligands, namely: meso-tetra-(4-carboxyphenyl)-porphyrin (TCPP), N-methylimidazole (N-Me-Im), 3-amino-1,2,4-triazole-5-carboxylic acid (ATZC), 2,2'-bis(4,5-dimethylimidazole) (bis-Me-Im), phenanthroline (phen), 2-pyrazinocarboxylic acid (CO₂-Pz), 3,6-di-2-pyridyl-1,2,4,5-tetrazine (DPTZ) and 2,4,6-tri(2-pyridyl)-s-triazine (TPTZ), adsorbed on a carbon substrate and submitted to thermal treatment. These ligands comprise five and six membered rings with one to four N-atoms. Key parameters such as the pyrolysis temperature, the complex load and the metal: ligand ratio were studied, in order to optimize the efficiency of the catalysts. The synthesized catalysts were characterized by several physical bulk and surface techniques, namely XRD, TGA, Raman spectroscopy, XPS, EDX and electron microscopies (SEM and TEM).

The best catalyst was obtained from a Cobalt-phenanthroline precursor, adsorbed on a mesoporous carbon material, and pyrolyzed at 700 °C. The equilibrium potential was 0.90 V vs NHE (1.0 V for Pt), exchange current density 25 $\mu\text{A cm}^{-2}$, Tafel slope was 90 mV dec⁻¹, and 4.0 exchanged electrons, less than 9% in H₂O₂ yield, and half wave potential only 80 mV lower than that of Platinum (10%). This catalyst exhibited the highest N content as determined by XPS.

The electrochemical data of the prepared catalysts were analyzed in the context of the TGA, XRD and XPS information. A correlation between ORR activity and the N content (XPS) was found. This result strongly supports the model that proposes N atoms as the active sites, and provides a rational tool for designing new catalysts.

©2015 Elsevier Ltd. All rights reserved.

1. Introduction

Fuel cells are promising energy conversion devices, they employ H₂ and O₂ (or air) avoiding the emission of greenhouse-gases [1–3]. Proton Exchange Membrane Fuel Cells (PEMFC) which operate at relatively low temperature (50–100 °C) require Platinum based catalysts for both the anodic and cathodic reactions [4,5]. The cathodic reaction (i.e. reduction of oxygen) is relatively slow and displays an appreciable overpotential, hence the amount

of Platinum employed in the cathode is high to compensate the low electrochemical activity [6,7]. Platinum is expensive and its availability is limited, and these facts have prevented the massive or large scale use of this technology, for example in electrical vehicles [8]. Platinum catalysts have an additional complication which is their strong sensibility towards CO traces present in H₂ gas (obtained by reforming) [9], and cross over effects (if methanol is used in the anode) [10]. This has led to an extensive research of Platinum-free or Non-Noble catalysts for the Oxygen Reduction Reaction (ORR) [11–13].

After the discovery in the 60's that Co-phthalocyanines catalyze the ORR [14], and inspired in the active site of the cytochrome C oxidase [15], which holds an Fe-heme active site, much work has

* Corresponding author. Tel.: +54-11-6772-7181; fax: +54-11-6772-7121.
E-mail address: roncaroli@cnea.gov.ar (F. Roncaroli).

been done employing Co and Fe complexes with macrocycles, like porphyrins and other nitrogenated ligands, as catalysts for the ORR [11–13]. Later, it was found that the pyrolysis products of these compounds, as well as other complexes obtained from Co and Fe salts, N-donor ligands and/or polymers, supported on different carbons displayed a higher activity and stability than their precursor materials, comparable in some cases to that of Platinum [16–18]. Recently, metal-free catalysts, consisting mainly in N-doped carbons (graphenes, nanotubes, carbon nitride, etc) have shown ORR activity which was even higher than that of Platinum in alkaline medium [19–21].

Although catalysts for ORR have been synthesized for decades [13–18], there is still a big debate about the ORR active site for Pt-free catalyst [22,23]. Three main models of the structure of the active site have been proposed: i) Fe-N₄ or Co-N₄ moieties bound to the graphite structure during thermal treatment [24]. ii) Metallic particles of Fe and Co generated during the pyrolysis, which are detectable through electron microscopies [25]. iii) Nitrogen atoms which are inserted in the graphitic structure through the pyrolysis of N-precursors, particularly metal complexes, or through physical methods like chemical vapor deposition, laser ablation, arc discharge, etc. [19–21].

The existence of metal-free catalysts, in other words, the fact that metals are not needed to catalyze the oxygen reduction reaction, is probably the strongest evidence supporting the idea that N-atoms are the actual active sites. There is a lot of controversy about which type of N-atoms correspond to the active site. Many authors propose that pyridinic-N atoms, which lay at the borders of the graphite layers, forming “zig-zag” structures at the edges, are the active sites [26]. Others, in contrast, propose pyrrolic-N or alternatively graphitic-N (quaternary-N) atoms as the active sites [27]. However in most cases, the presence of metals during the synthesis, or after it, is necessary to reach a higher ORR activity. The presence of the metal would facilitate the incorporation of N-atoms during the pyrolysis in the proper conformation [28]. Some authors synthesized metal-free catalysts employing metal complexes or, more recently, metal organic frameworks (MOFs), followed by acid leaching, but traces of metal may be still present in the final product [29–31]. Moreover, in many cases, the acid treatment performed after the pyrolysis to remove unwanted or unreactant metallic particles, produces a reduction of the ORR activity. All these evidences makes very difficult to decide whether, metal- or N-atoms, correspond to the active sites.

Independently from the mechanism or the nature of the active site, experimental evidences have shown that: the nature and amount of metal employed, pyrolysis temperature, carbon support, N-rich polymer- and/or ligand-structure are key parameters that determine the ORR activity of these catalysts [18–28].

In the present work, we present a systematic study on the influence of the nitrogenated ligand in the precursor complex on the ORR activity. Several Fe and Co complexes were prepared with different N-heterocyclic ligands. These ligands comprise five and six membered rings with one to four N-atoms (see Fig. 1). In a first part of this report, the catalysts were characterized by several physical and spectroscopic techniques. In the second part, a detailed electrochemical study was performed. Correlating the electrochemical data with the physical characterization, it was possible to conclude which structural parameters of the precursor ligand are relevant for ORR. In a final attempt to further improve these materials and reach a catalytic activity closer to that of Platinum, a mesoporous carbon material was tested as support for some of the catalysts. Due to its pore size distribution this carbon material has a larger surface area than Vulcan XC carbon, offering a larger catalyst adsorption surface area and better mass transport.

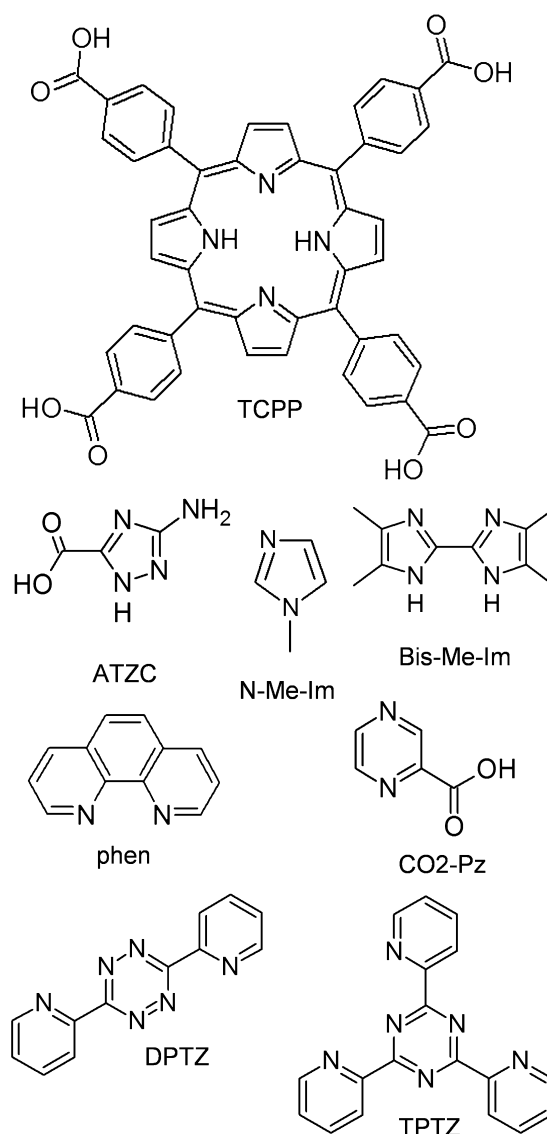


Fig. 1. Structures of the ligands employed for catalysts preparation and abbreviated names used within the text. Complete names are given in the experimental section.

2. Experimental

2.1. Chemicals and catalyst preparations

2.1.1. Chemicals

All chemicals were analytical grade and used without further purification. Ligands employed for the catalysts synthesis are depicted in Fig. 1. Cobalt meso-tetra-(4-carboxyphenyl)-porphyrin (CoTCPP) was from Porphyrin Systems GbR (Germany). N-methylimidazole (N-Me-Im), 3-amino-1,2,4-triazole-5-carboxylic acid (ATZC), 2,2'-bis(4,5-dimethylimidazole) (bis-Me-Im), phenanthroline (phen), 2-pyrazinecarboxylic acid (CO₂-Pz), 3,6-di-2-pyridyl-1,2,4,5-tetrazine (DPTZ) and 2,4,6-tri(2-pyridyl)-s-triazine (TPTZ) were purchased from Sigma-Aldrich. Cobalt Chloride hexahydrate, Ferrous Sulfate heptahydrate and concentrated Sulfuric Acid were from Merck. Co₃O₄ was provided by Mallinckrodt. Nitrogen (99.998 %) and Oxygen (99.5 %) were supplied by Indura S.A. (Argentina). Isopropyl alcohol was from Biopack. Nafion solution in isopropanol was purchased from Ion Power, Inc. (USA) (Liquion solution LQ1115 1100 EW 15%). Water was purified through an Arium Pro equipment from Sartorius until a specific

conductivity of $18 \text{ M}\Omega \text{ cm}^{-1}$. Vulcan XC-72 carbon (CABOT) was purified by washing with hydrochloric acid 0.5 M (35°C) to remove metallic or cationic impurities. Pt supported on Vulcan XC-72 catalyst was obtained from ETEK.

2.1.2. Mesoporous carbon preparation

A structured carbon material was used as support for some of the synthesized Cobalt complexes. The surface area (BET) of this material is $470 \text{ m}^2 \text{ g}^{-1}$. The preparation and characterization has already been described in a previous report from our group [32]. The carbon material in a powder form was grinded and passed through a $40 \mu\text{m}$ pore sieve.

2.1.3. Catalysts preparation

The precursor materials were prepared following a similar procedure to previous reports [26,29,33]. In general, 40 mg of $\text{CoCl}_2 \cdot 6\text{H}_2\text{O}$ were dissolved in 3.0 ml of water. To the pink $[\text{Co}(\text{H}_2\text{O})_6]^{2+}$ solution thus obtained, a four-fold molar excess of the mono dentate ligands (i.e. ATZC, N-Me-Im [34] and $\text{CO}_2\text{-Pz}$ [35]) or a two-fold molar excess of the bidentate ligands (i.e. bis-Me-Im [36], phen [37] and DPTZ) was added. The mixture was set in the ultrasonic bath during $30 - 60$ minutes. The formation of the complexes was evidenced by color changes and precipitate formation in some cases, which were in agreement with available literature. Completely soluble complexes were obtained with the ligands: N-Me-Im (blue) [34] and phenanthroline (orange) [37], or suspensions of insoluble complexes were alternatively obtained with other ligands: ATZC (pink), $\text{CO}_2\text{-Pz}$ (yellow-orange) [35], bis-Me-Im (orange) [36], and DPTZ (black).

The FeCo(TPTZ) complex was prepared using 20 mg of $\text{CoCl}_2 \cdot 6\text{H}_2\text{O}$, 24 mg $\text{FeSO}_4 \cdot 7\text{H}_2\text{O}$ and 104 mg of ligand, what afforded a dark blue solution [33,38]. Phenanthroline catalysts were prepared using only Co (40 mg $\text{CoCl}_2 \cdot 6\text{H}_2\text{O}$), or only Fe (44 mg $\text{FeSO}_4 \cdot 7\text{H}_2\text{O}$) or a mixture of both metals (20 mg of $\text{CoCl}_2 \cdot 6\text{H}_2\text{O}$ and 24 mg $\text{FeSO}_4 \cdot 7\text{H}_2\text{O}$), affording deep red solutions when Fe was present [39].

The influence of the molar ligand / metal ratio was investigated with phenanthroline, using one, two and three moles of ligand respect to Co.

100 mg of carbon (Vulcan or mesoporous carbon) were added to the complex solutions or suspensions described above. For the CoTCP derived catalysts, 20 mg of complex and 50 mg of Vulcan were used. The mixture thus obtained was set in an ultrasonic bath during 2 hours to allow adsorption of the corresponding complex and subsequently allowed to stand overnight at room temperature. Evaporation to dryness was achieved at maximal temperature of 70°C in a vacuum oven to avoid desorption of the complexes. The raw product was grained, mixed and submitted to pyrolysis at 500°C , 700°C or 900°C during 2 hours, under Nitrogen (flow 1 l h^{-1}), using an Indef T300 tubular electric furnace at a heating rate of $10^\circ\text{C min}^{-1}$.

The influence of the complex load was studied with phenanthroline. For this purpose 80 mg of $\text{CoCl}_2 \cdot 6\text{H}_2\text{O}$, 140 mg of phenanthroline (or 168 mg $\text{CO}_2\text{-Pz}$) and 100 mg of carbon were used. These catalysts are labeled "X2" in Tables and Figures.

For comparison in the spectroscopic studies, a sample of the $[\text{Co}(\text{phen})_3]\text{Cl}_2$ complex was prepared dissolving $\text{CoCl}_2 \cdot 6\text{H}_2\text{O}$ and 3 equivalents of phenanthroline in water. The solution was stirred during two hours under N_2 and the color changed from pink to intense orange, in agreement with literature data [37,40,41]. The presence of Co(II) and coordination of the ligand was checked by XPS [40,41].

2.1.4. Ink preparation

10 mg of the catalyst were suspended in 180 mg of isopropyl alcohol and set in the ultrasonic bath for 15 minutes. $30 \mu\text{l}$ of

Nafion (5% in isopropyl alcohol IonPower) were added. $10 \mu\text{l}$ of the ink thus prepared (0.5 mg catalysts) were spread on the 0.196 cm^2 gold disk and employed in the electrochemical experiments.

2.2. Physical characterization

2.2.1. XRD

Powder X-ray diffraction patterns were measured using an Empyrean diffractometer equipped with a PixCel 3D detector, $\text{CuK}\alpha$ 40 mA 40 kV radiation source, and with angle range $10^\circ < 2\theta < 90^\circ$, employing a 0.02° step size and a 4 s step time.

2.2.2. TGA

Thermogravimetric Analysis curves were recorded on a Shimadzu TGA 50, employing approximately 2.5 mg of sample, under a N_2 flow of 20 ml min^{-1} and a heating rate of $10^\circ\text{C min}^{-1}$. Samples were prepared analogously to the catalysts.

2.2.3. XPS

X-ray photoelectron spectra were recorded under ultra-high vacuum conditions with a PHI VersaProbe II spectrometer, using Al $\text{K}\alpha$ radiation, equipped with a 150 mm radius hemispherical electron energy analyzer and a 16 channels detector. Binding energies were referred to the C 1s signal at 285 eV .

2.2.4. Raman

Spectra were recorded on a LabRAM HR Raman system (Horiba Jobin Yvon), equipped with two monochromator gratings and a charge coupled device detector. A 1800 gmm^{-1} grating and a 100 mm hole result in a spectral resolution of 1.5 cm^{-1} . The spectrograph is coupled to an imaging microscope with $10\times$, $50\times$, and $100\times$ magnifications. The He-Ne laser line at 632.8 nm was used as excitation source and was filtered to give a laser power or density at the exit of the objective lens varying from 0.1 to 1 W mm^{-2} . Several measurements were performed, adjusting the laser fluence, to ensure that heating produced by the laser was minimized and that the sample was not altered. Measurements were taken in a backscattering geometry, with $10\times$ and $50\times$ magnifications.

2.2.5. SEM/EDX/TEM

Catalyst morphology was characterized by scanning electron microscopy (SEM) on a FEI Quanta 400 microscope or a Carl Zeiss NTS-SUPRA 40, both instruments afforded the Energy-Dispersive X-ray spectra (EDX). Transmission electron microscopy (TEM) images were acquired with a Philips CM200 microscope.

2.3. Electrochemical characterization

2.3.1. Electrochemical measurements

All electrochemical experiments were performed employing an Autolab PGSTAT302N potentiostat (Echochemie, Netherlands). For cyclic voltammetry and RRDE (Rotating Ring Disc Electrode) experiments, the Autolab potentiostat was coupled to a rotating ring disk electrode (Pine Research Inst.; Raleigh, NC). A Ag/AgCl (KCl saturated) reference electrode was used for all the electrochemical experiments and the potentials in this work were referred to the Normal Hydrogen Electrode (NHE). The counter electrode was a large area rolled gold wire. A three electrodes electrochemical cell with a jacket was employed, and its temperature was kept at $25 \pm 0.5^\circ\text{C}$ by circulating a thermostated liquid using a Techne temperature controller.

Oxygen Reduction Reaction (ORR) experiments were performed using a rotating gold disk electrode (0.196 cm^2) – platinum ring electrode (Pine Research Inst.). All the experiments were performed in 0.5 M H_2SO_4 aqueous solution. Voltammograms

were recorded for the ORR at different rotation speed ($\omega = 100$ –2500 rpm). The potential was scanned between 1.1 and 0 V (vs. NHE) at 5 mVs^{-1} . The ring potential was fixed at 1.4 V (vs. NHE) in order to oxidize the H_2O_2 generated in the disk. The calibration of the RRDE was carried out by measuring the disk and ring currents in a $0.005 \text{ M K}_3\text{Fe}(\text{CN})_6 + 0.1 \text{ M K}_2\text{SO}_4$ electrolyte. The disk potential was cycled between 0.0 and 1.1 V (vs. NHE) at 5 mVs^{-1} while the ring potential was fixed at 1.4 V (vs. NHE) in order to oxidize the $[\text{Fe}(\text{II})(\text{CN})_6]^{4-}$ generated on the disk. This procedure was repeated at different rotating speeds. The RRDE collection efficiency (N) was determined from the slope of disk current (I_D) vs. ring current (I_R) plots, affording $N = 0.180 \pm 0.005$.

2.3.2. Data analysis

Efficiency parameters, i.e. Tafel slopes, equilibrium potential (E_{eq}) and exchange current density (j_o) were calculated by means of Tafel plots (see Table 2 and Fig. SI 3) using the Nova 1.10 program. E_{eq} and j_o were determined from the intercept of the two trend lines corresponding to the ORR and the anodic process (Fig. SI 3). j_o was calculated considering a geometrical area of the electrode, namely 0.196 cm^2 . Errors in these parameters correspond to the standard deviation of several measurements.

The number of electrons transferred per molecule of reduced O_2 , n_{e-} , was determined through Koutecky–Levich plots (K-L). The overall measured current density, j , of the ORR can be expressed in terms of the kinetic current density, j_k , and the diffusion limited current density, j_d , by the Koutecky–Levich (K-L) equation (1) [42].

$$\frac{1}{j} = \frac{1}{j_k} + \frac{1}{j_d} = \frac{1}{j_k} + \frac{1}{B\omega^{1/2}} \quad (1)$$

$$B = 0.2n_eFC_oD_o^{2/3}\nu^{-1/6} \quad (2)$$

In equation (2), 0.2 is a constant used when the rotation speed, ω , is expressed in rpm, F the Faraday constant ($96485 \text{ A s mol}^{-1}$), C_o is the concentration of dissolved oxygen ($1.1 \times 10^{-6} \text{ mol cm}^{-3}$), D_o is the diffusion coefficient of oxygen in the solution ($1.4 \times 10^{-5} \text{ cm}^2 \text{ s}^{-1}$), and ν the kinematic viscosity of the $0.5 \text{ M H}_2\text{SO}_4$ solution ($1.0 \times 10^{-2} \text{ cm}^2 \text{ s}^{-1}$), all of them at 298 K [42]. The inverse of the slope in the K-L plot, B , is proportional to n_{e-} , and allowed to calculate this last parameter.

The yield in hydrogen peroxide, H_2O_2 can be calculated from equation (3)

$$\% \text{H}_2\text{O}_2 = \frac{200I_R/N}{I_D + I_R/N} \quad (3)$$

where I_R and I_D are the ring and the disk currents respectively, and N is the experimental collection efficiency (0.180 ± 0.005) [42].

2.3.3. Cell Performance

Pt supported over Vulcan carbon (Pt/V) 20 % w/w (E-Tek) was used as the anode catalyst, while the prepared catalysts (Co(CO₂Pz) Vulcan 700 °C, Co(phen) Vulcan °C and Co(phen) meso 700 °C) were used as cathode catalyst. The electrodes were prepared as follows. The catalyst suspension comprising approximately 100 mg catalyst with 1.0 g isopropanol and 200 mg Nafion ionomer solution (5 % w/w, Ion Power), was spread on one side of a 5.0 cm^2 Toray C paper TGP-H 60 10 % PTFE coated (Fuel Cell Technologies). The Pt catalysts loading was 9–19 mg, while the Co catalyst loading was 26–71 mg. A Nafion 212 membrane (Ion Power) was placed between the electrodes and then hot pressed at $150 \text{ }^\circ\text{C}$ and 40 bar for 25 min. The Nafion membrane was previously treated by boiling in H_2O_2 3 % w/w (H_2O_2 30 % w/w, Biopack) followed by H_2SO_4 3 % w/w (95–97 % w/w, Merck). After assembling the cell, the MEA was re-humidified by circulating water overnight at $80 \text{ }^\circ\text{C}$. Humidified H_2 (RG 4.8, Indura) and O_2 (RG 4.8, Indura)

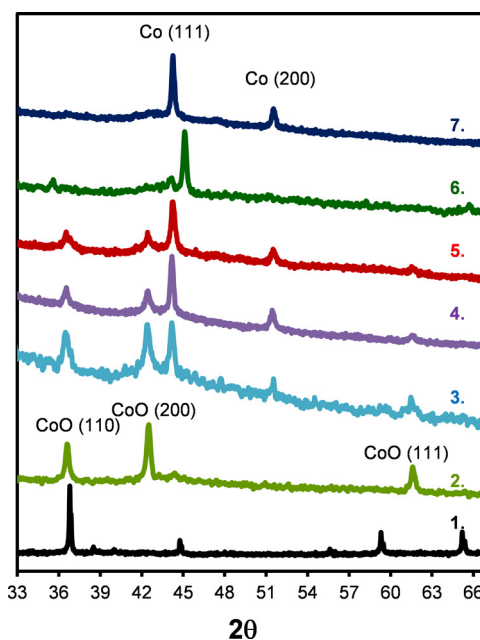


Fig. 2. X-Ray diffraction patterns of selected catalysts and reference compounds: 1. Co_3O_4 , 2. CoCl_2 Vulcan $700 \text{ }^\circ\text{C}$, 3. Co(ATZC) Vulcan $700 \text{ }^\circ\text{C}$, 4. Co(bis-Me-Im) Vulcan $700 \text{ }^\circ\text{C}$, 5. Co(CO₂Pz) Vulcan $700 \text{ }^\circ\text{C}$, 6. FeCo(TPTZ) Vulcan $700 \text{ }^\circ\text{C}$, 7. Co(phen) Vulcan $700 \text{ }^\circ\text{C}$.

were circulated at the anode and cathode, respectively, at different flow rates. Galvanodynamic polarization tests were performed at $90 \text{ }^\circ\text{C}$ from the open circuit voltage (OCV) to a voltage close to short circuit (0.05 V). The measurements were performed using a University Test Station system from Fuel Cell Technologies.

3. Results and discussion

3.1. Physical characterization

3.1.1. XRD

Catalysts were characterized through powder XRD, some of them are shown in Fig. 2 and SI 1. Upon pyrolysis at $500 \text{ }^\circ\text{C}$ these materials were mainly amorphous and only weak signals in the diffractogram were detected. After pyrolysis at $700 \text{ }^\circ\text{C}$ sharp patterns were observed. They were assigned to CoO and Co phases, no other components were detected, particularly Co_3O_4 [43]. From the signal intensities, it was possible to conclude that catalysts obtained from six membered ring ligands, i.e. phen, CO₂-Pz, TPTZ and DPTZ, had the lowest contents in CoO. In contrast, using five membered ring ligands, i.e. ATZC and bis-Me-Im, catalysts with higher CoO content were obtained. When no ligand was added in the preparation, (i.e. CoCl_2 on Vulcan), the catalyst contained mainly CoO and no Co was detected.

Samples which were submitted to thermal treatment at $900 \text{ }^\circ\text{C}$ showed an increase in the amount of CoO. It is not clear whether the source of oxygen are traces of this gas present in the furnace or oxygenated groups (OH, carboxylates, oxo groups) present in the Vulcan substrate.

3.1.2. TGA

In order to gain insight into the reactions that occur during the pyrolysis process, thermogravimetric curves were obtained using selected ligands, under similar conditions to those of the synthesis (see Fig. 3). An initial small weight loss observed for some samples until $150 \text{ }^\circ\text{C}$, is interpreted in terms of water evaporation. This is followed by a second sharp decay in the weight, interpreted as volatilization of ligand weakly coordinated to the metal ions or

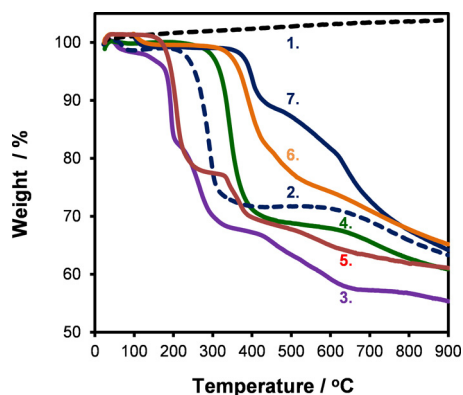


Fig. 3. Thermogravimetric analysis of selected catalyst precursors: 1. Vulcan, 2. Phenanthroline on Vulcan, 3. Co(ATZC) on Vulcan, 4. Co(bis-Me-Im) on Vulcan, 5. Co(CO₂Pz) on Vulcan, 6. FeCo(TPTZ) on Vulcan, 7. Co(phen) on Vulcan, obtained under N₂ flow of 20 ml min⁻¹ and a heating rate of 10 °C min⁻¹.

weakly adsorbed to the carbon support [28]. The temperature at which this process starts, depends on the nature of the ligand, being highest for Co(phen) Vulcan, and lowest for Co(ATZC) Vulcan. The fast weight loss is followed by several decays with smaller slopes that start between 300–500 °C, this is probably due to reaction of functional groups within the carbon matrix, volatilization of metal coordinated ligands, ligand condensation with the carbon matrix and carbon graphitization [44]. The curve for Co(phen) is shifted to much higher temperatures when compared with the curve for the ligand alone adsorbed on the same substrate, evidencing the formation of an appreciable stable metal-complex. Hence, it is possible to conclude that the presence of metal ions increases the ligand (and consequent nitrogen) retention during the pyrolysis [28]. This has been proposed to play a determinant role in the catalytic activity (*vide infra*) [28]. The relatively low temperature weight loss observed for the ATZC and CO₂Pz derived materials, is probably induced by decarboxylation and decomposition of the ligand. It is possible to observe in Fig. 3 that phenanthroline and TPTZ are the most retained studied ligands.

3.1.3. Raman

Fig. 4 shows the Raman spectra for some phenanthroline derived catalysts. Analogous spectra obtained employing other ligands were also measured obtaining similar results (not shown). The spectra of the pyrolyzed samples (500 and 700 °C) are dominated

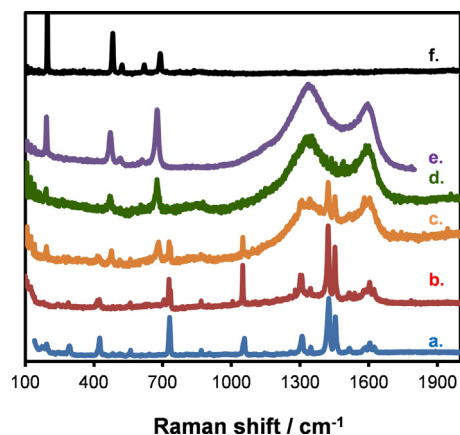


Fig. 4. Raman spectra of selected catalysts and some reference compounds: a. Co(phen)₃Cl₂, b. Co(phen) Vulcan without pyrolysis, c. Co(phen) Vulcan 300 °C, d. Co(phen) Vulcan 500 °C, e. Co(phen) Vulcan 700 °C, f. Co₃O₄.

by two bands at 1332 cm⁻¹ and 1590 cm⁻¹. The first signal, called D band, is present in all graphite-like carbons and originates from structural defects and sp³ carbons. The second signal, called G, is assigned to the E_{2g} stretching vibrations in the basal plane of graphite [45].

Other signals at 192 cm⁻¹, 472 cm⁻¹, 514 (weak) cm⁻¹, 610 (weak) cm⁻¹ and 676 cm⁻¹ are also present in the spectrum of the sample heat-treated at 700 °C, and cannot be assigned to the Co(phen) precursor complex. The Raman spectrum of CoO is reported to exhibit four bands at 468 cm⁻¹, 510 cm⁻¹ (weak), 605 cm⁻¹ (weak), and 672 cm⁻¹ [46]. The spectrum of Co₃O₄ (shown in Fig. 4) shows bands at 482 cm⁻¹, 522 cm⁻¹ (weak), 620 cm⁻¹ (weak) and 689 cm⁻¹. From this data, we assign these bands in the pyrolyzed sample to CoO or to a mixture of CoO/Co₃O₄ generated on the surface of the particles. The presence of CoO is in agreement with the XRD patterns. Signals from the precursor complex could be detected after thermal treatment at 300 °C in agreement with the TGA analysis.

3.1.4. XPS

Fig. 5 shows the high resolution XPS spectra of some selected catalysts (survey scan spectra are shown in the Supplementary Information). Deconvolution of the N1s XPS spectra was done using three subpeaks centered at 399.3 ± 0.2 eV, 400.8 ± 0.4 eV and 402.5 – 403.5 eV, assigned, according to literature, to: Co-coordinated N (399–400 eV), Pyrrolic-N (400–401 eV), Graphitic-N (401–402 eV) and Oxygenated-N (402–405 eV) [47–49]. Pyrrolic-N refers to the nitrogen atom on the edge of graphite planes with two adjacent carbon atoms. It has one lone pair of electrons in addition to the one electron donated to the conjugated bond system, imparting Lewis basicity to the carbon. Graphitic-N, which is also termed as “Quaternary-N”, represents the nitrogen atom bonded to three carbon atoms within a graphite (basal) plane, while Pyrrolic groups refer to nitrogen atoms that contribute to the π system with two π electron within a five-membered ring. Finally, Oxidized-N corresponds to N bound to O (N⁺-O⁻). From our spectra it is difficult to distinguish between Pyrrolic-N and Graphitic-N. Oxidized-N was also detected, although in lower concentration. In Fig. 5, the corresponding spectrum of the Co(phen)₃Cl₂ complex is shown, displaying a single band centered at 399.3 eV. The N1s XPS spectrum of the as received phenanthroline shows a band centered at 398.8 eV, hence we conclude that the Co-coordinated nitrogen corresponds to Pyrrolic-N. In the same Figure, it is possible to observe that, after thermal treatment, a similar ratio between Pyrrolic-N and Pyrrolic-N is reached, independently of precursor ligand.

The signals shown in the region around 781 eV in Fig. 5, correspond to the Co 2p_{3/2} binding energy spectra. They were deconvoluted into the following sub-spectra centered at: 779.3 ± 0.3 eV, 780.0 ± 0.3 and 781.8 ± 0.4 eV, which can be assigned to Co₃O₄ (779.4 eV), CoO (780 eV) and Co coordinated to N respectively (781.8 eV), according to literature data [47–50]. The Co(phen) and Co(TPTZ) derived catalysts displayed a band at 781 eV which is tentatively assigned to CoO. The Co(phen)₃Cl₂ complex shows a band at 781.9 eV and a band at 780.2 eV. A signal centered at 781.6 eV has been observed in the [Co(III)(NH₃)₆](Br)₃ complex [40], while a binding energy at 780.4 eV was measured for the Co 2p_{3/2} level in the [Co(II)(terpyridine)(bipyridine)Cl]Cl complex [41]. Bands assignable to metallic Co (778 eV) [47–50] were not detected in any sample. From these findings, we conclude that the CoO and metallic particles observed in the diffractograms must be covered with different amounts of oxides, being these compounds partially or totally coordinated on their surfaces to nitrogen (pyridinic-N).

Table 1 shows the catalyst compositions (% weight) obtained from XPS spectra, together with data obtained from EDX.

Table 1
Element compositions for selected catalysts (% weight) obtained from EDX and XPS spectra.

Catalysts	EDX				XPS						
	C	O	Co	Cl	S	C	O	Co	N	Cl	S
Co(phen) Vulcan 500 °C						84.6	5.0	6.7	3.7		
Co(phen) Vulcan 900 °C						91.0	4.6	3.3	0.3	0.8	
Co(phen) meso 900 °C						80.3	9.4	4.8	5.5		
Co(phen) x2 meso 700 °C ^a	81.1	8.8	9.4	0.7		76.7	9.0	6.8	7.5		
Co(phen) x2 Vulcan 700 °C ^a	86.0	2.9	10.3	0.8		80.1	7.8	6.1	6.0		
Co(phen) meso 700 °C	86.7	7.3	6.0			81.2	7.8	4.0	7.0		
Co(phen) Vulcan 700 °C	90.0	3.2	6.0	0.4	0.4	80.9	5.9	5.8	6.9	0.5	
FeCo(TPTZ) Vulcan 700 °C	88.9	4.9	5.4 ^b	0.3	0.5	78.7	8.9	4.2	7.5	0.7	
Co(CO ₂ Pz) Vulcan 700 °C	90.2	4.3	5.2		0.3	79.3	11.6	4.1	5.0		
Co(bis-Me-Im) Vulcan 700 °C	93.1	3.4	2.9	0.1	0.5	90.1	3.2	2.8	3.1	0.3	0.5
Co(ATZC) Vulcan 700 °C	92.8	2.1	4.7		0.4	92.3	2.1	3.4	2.1	0.1	
Phen Vulcan 700 °C						84.6	13.8		1.6		

^a X2 means double complex load.

^b Fe+Co content.

Differences between the values obtained through this two techniques can be ascribed to a different element distribution on the particle surfaces (XPS) from that in the bulk (EDX). There is a higher content of N and O on the surface than in bulk, actually, no N could be detected by EDX in any sample. In contrast, Co content is higher in bulk, than on surface. It has been observed that Co particles are sometimes buried or encapsulated within the carbon matrix [25]. A decrease in N content is observed as the pyrolysis temperature is increased, this is particularly evident with the samples obtained at 900 °C, in agreement with our TGA data and previous reports [51]. Phenanthroline and TPTZ derived catalysts reached the highest N content when compared with the other studied ligands (ATZC, bis-Me-Im and CO₂Pz), also in agreement with the ligand retention observed by TGA. In the case of Co(phen) derived catalysts, the N content could be further increased using the mesoporous carbon as substrate and duplicating the initial complex load (x 2 in Table 1) reaching 7.5 %. This data will be discussed in the context of the electrochemical characterization.

3.1.5. Electron microscopy

SEM images of the Co(phen) derived catalysts supported on Vulcan revealed carbon particles of approximately 200 nm composed of aggregates of smaller almost spherical particles of approximately 40 nm (Fig. 6 a, b), leaving hollow pores of the same size between the particles. In contrast the analogous catalyst supported on the mesoporous carbon is formed by much larger carbon particles of approximately 1 μm size, with pores of 40 nm diameter (Fig. 6 A, B), as expected from its synthetic procedure [32]. The composition was determined through the EDX spectra and the electron back scattered images (Fig. 6 c, C) which shows

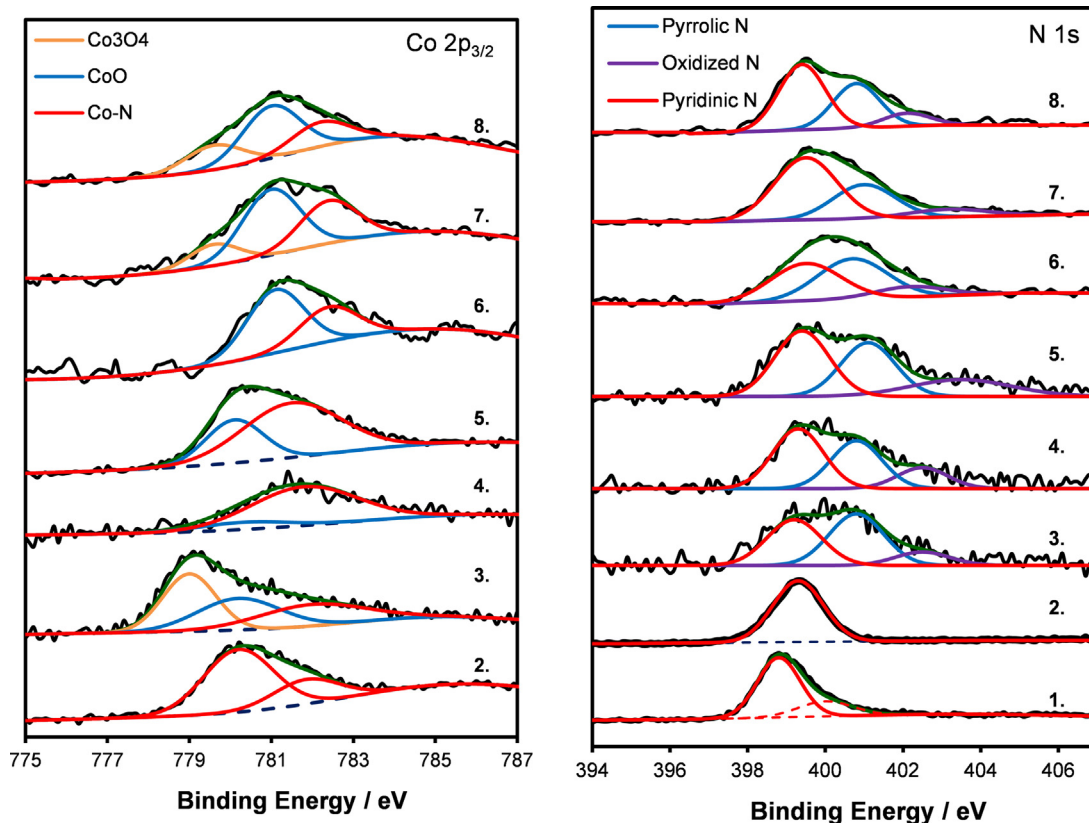


Fig. 5. High resolution XPS spectra in the Co 2p_{3/2} and N 1s region for some selected catalysts and reference compounds: 1. Phenanthroline, 2. Co(phen)₃Cl₂, 3. Co(ATZC) Vulcan 700 °C, 4. Co(bis-Me-Im) Vulcan 700 °C, 5. Co(CO₂Pz) Vulcan 700 °C, 6. FeCo(TPTZ) Vulcan 700 °C, 7. Co(phen) Vulcan 700 °C, 8. Co(phen) meso 700 °C. Simulations were done using Gaussian line shapes and are shown in color. Solid black lines correspond to experimental spectra.

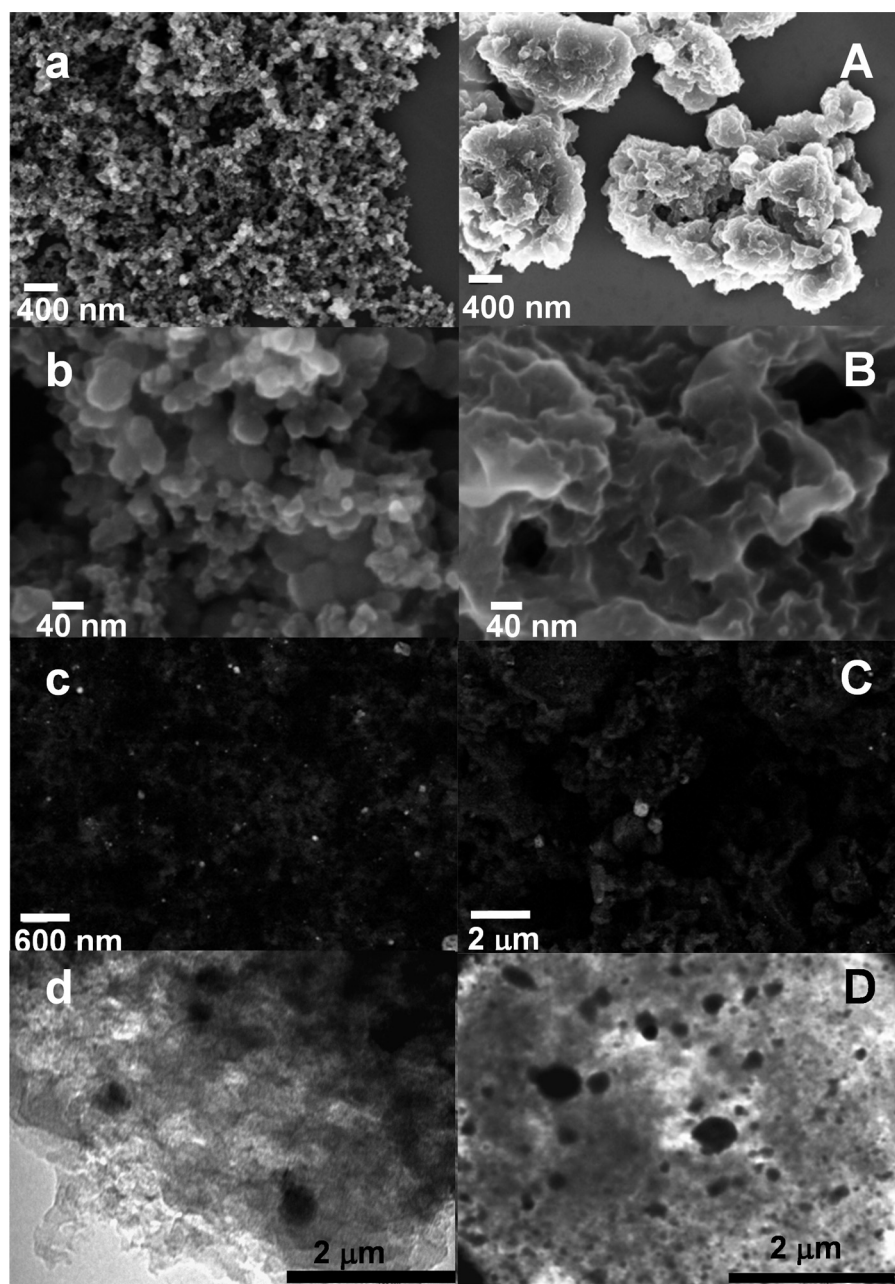


Fig. 6. Micrographs of Co(phen) based catalysts (pyrolyzed at 700 °C). a – d supported on Vulcan carbon, A – D supported on mesoporous carbon. a – b and A – B secondary electron SEM images with different magnification. c and C electron backscattered SEM images. d and D TEM images.

bright areas for Co/CoO/Co₃O₄ particles and dark ones for the carbon matrix. With this last technique, Co particles of 0.1 – 1.0 μm diameter were observed on both supporting materials. Similar results were obtained employing ATZC, bis-Me-Im CO₂-Pz and TPTZ as ligands in the preparation of the catalysts.

Fig. 6 D also shows the TEM image of the Co(phen) meso 700 °C catalysts, where large Co/Co_xO_y particles (size around 500 nm) can be observed, in agreement with the SEM data, but also particles smaller than 50 nm could be detected.

3.2. Electrochemical characterization

3.2.1. ORR analysis by RRDE

Fig. 7 shows the cyclic voltammetry for the Co(CO₂Pz) Vulcan 700 °C catalysts in both O₂- and N₂- saturated 0.5 M H₂SO₄ solutions. It is possible to observe a peak at ca 0.7 V assignable to

the electro-catalytic Oxygen Reduction Reaction (ORR), not observed under N₂ saturation. Similar plots were obtained with the other catalysts. Fig. 8 shows typical steady-state polarization curves at different rotation rates in an O₂-saturated 0.5 M H₂SO₄ solution for the Co(phen) derived catalyst supported on a mesoporous carbon obtained at 700 °C. Analogous plots for other prepared materials are shown in the SI. Fig. 9 shows the linear sweep voltammograms obtained on a rotating disk electrode at 2500 rpm for selected catalysts. The corresponding curve for Platinum 10 % adsorbed on Vulcan carbon is also shown for comparison. This data is summarized in Table 2 together with the Tafel slopes, exchange current densities (j_0), number of exchanged electrons (n_{e^-}) and yields in H₂O₂.

Linear sweep voltammograms obtained at different rotation rates, using equations (1) – (2), afforded Koutecky-Levich plots (K-L) which are shown in the SI. Fig. 10 shows the K-L plot for some

Table 2
Electrokinetic parameters and H₂O₂ yield for the synthesized catalysts.^a

Catalyst	E_{eq} (v vs NHE) ^b	j_o ($\mu\text{A cm}^{-2}$) ^{b,c}	Tafel slope (mV dec^{-1}) ^b	n_{e-} ^d	% H ₂ O ₂ ^e
Co(DPTZ) Vulcan 500 °C	0.92 ± 0.02	18 ± 2	260 ± 20		
Co(N-Me-Im) Vulcan 500 °C	0.96 ± 0.05	12 ± 2	240 ± 40		
Co(ATZC) Vulcan 500 °C	0.91 ± 0.02	30 ± 0.4	230 ± 20		
FeCo(TPTZ) Vulcan 500 °C	0.93 ± 0.02	30 ± 9	240 ± 10		
Co(CO ₂ -pz) Vulcan 500 °C	0.93 ± 0.02	6 ± 1	200 ± 10		
Co(phen) Vulcan 500 °C	0.96 ± 0.05	10 ± 2	180 ± 10		
Phen Vulcan 700 °C	0.88 ± 0.03	4.7 ± 0.3	113 ± 3		
CoCl ₂ Vulcan 700 °C	0.89 ± 0.02	6 ± 2	160 ± 20		20–40
Co(ATZC) Vulcan 700 °C	0.88 ± 0.02	23 ± 3	170 ± 10	2.9–3.5	5–42
Co(bis-Me-Im) Vulcan 700 °C	0.90 ± 0.02	10 ± 5	130 ± 5	2.7–3.0	15–35
Co(DPTZ) Vulcan 700 °C	0.88 ± 0.02	4 ± 2	100 ± 10	3.1–3.9	5–45
Co(TCPP) Vulcan 700 °C	0.90 ± 0.02	20 ± 5	105 ± 5	3.7–3.9	8–16
Co(CO ₂ -pz) Vulcan 700 °C	0.90 ± 0.05	10 ± 1	105 ± 6	3.9–4.0	8–12
FeCo(TPTZ) Vulcan 700 °C	0.92 ± 0.01	10 ± 2	95 ± 5	3.9–4.1	8–14
Co(phen) Vulcan 700 °C	0.90 ± 0.01	10 ± 3	85 ± 5	3.8–4.0	6–13
Co(phen) meso 700 °C	0.92 ± 0.05	11 ± 5	95 ± 10	3.9–4.1	10–12
Co(phen) x2 Vulcan 700 °C ^f	0.92 ± 0.02	15 ± 5	90 ± 10	3.8–4.1	4–8
Co(phen) x2 meso 700 °C ^f	0.90 ± 0.01	25 ± 2	90 ± 5	4.0–4.1	5–9
Fe(phen) Vulcan 700 °C	0.92 ± 0.01	9 ± 2	125 ± 5	3.8–4.0	4–8
FeCo(phen) Vulcan 700 °C	0.93 ± 0.02	16 ± 4	117 ± 7	3.8–3.9	6–10
Co(phen) Vulcan 900 °C	0.92 ± 0.02	2.0 ± 0.2	140 ± 10		15–40
Co(phen) meso 900 °C	0.95 ± 0.02	2.0 ± 0.5	90 ± 5		10–30
Pt 10 % Vulcan	0.97 ± 0.02	25 ± 2	85 ± 7		
Pt 20 % Vulcan	0.99 ± 0.02	60 ± 8	85 ± 7	3.9–4.1	0.5–1

^a For data analysis and catalysts synthesis, see experimental section. Steady-state ORR polarization curves, Koutecky-Levich plots and H₂O₂ yields of different catalysts are shown in the Supplementary Information.

^b From Tafel plots, see experimental section and Fig. S1 3.

^c j_o was calculated considering the geometrical area of the electrode (0.196 cm²).

^d From Koutecky-Levich plots (see SI).

^e from RRDE data, using equation (3).

^f X2 double complex load.

selected catalysts at 0.4 V vs NHE. From the slopes of these plots the numbers of exchanged electrons (n_{e-}) were obtained (equation (2)), which are shown in Table 2.

Analyzing the current densities obtained with the RRDE using equation (3) yields in H₂O₂ were obtained for most of the prepared catalysts (Table 2 and SI). Fig. 11 shows the % H₂O₂ as a function of the applied potential for some selected catalysts.

The best materials were obtained upon thermal treatment at 700 °C in comparison to 500 °C and 900 °C, as previously observed in several reports (see Table 2) [26,28,33]. Samples obtained at 900 °C, showed higher CoO content (XRD), and decreased N content (XPS).

Poly-pyridinic ligands are apparently the best ones to be used as precursors for catalysts, i.e. CO₂-Pz, and particularly phenanthroline and TPTZ, (the two last ones have been subject of some reports) [26,33]. These catalysts display the highest half wave

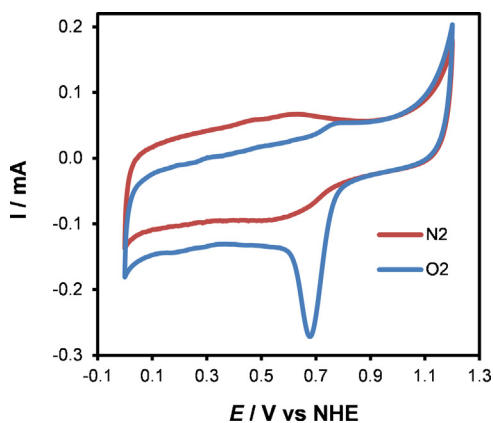


Fig. 7. Cyclic voltammety of the Co(CO₂Pz) Vulcan 700 °C catalysts supported on a gold disk, in N₂- or O₂-saturated 0.5 M H₂SO₄ solution, 25 °C, scan rate 5 mV s⁻¹.

potentials (as shown in Fig. 9), lowest Tafel slopes (95 – 105 mV dec⁻¹, see Table 2), n_{e-} values close to the ideal value of four electrons (Fig. 10) and the lowest H₂O₂ yields (< 15 %, Fig. 11). The FeCo(TPTZ) catalyst has been reported to have a low H₂O₂ yield [33], in agreement with our results. For the phenanthroline derived catalyst, the optimum Co:phen molar ratio probed to be 1:2. Increasing this ratio to 1:3 did not show appreciable improvements (see Fig. S1 4). These catalysts also show lower content in CoO (see Fig. 2, XRD). Phenanthroline and TPTZ are the most retained ligands during thermal treatment (TGA), and produce the catalysts

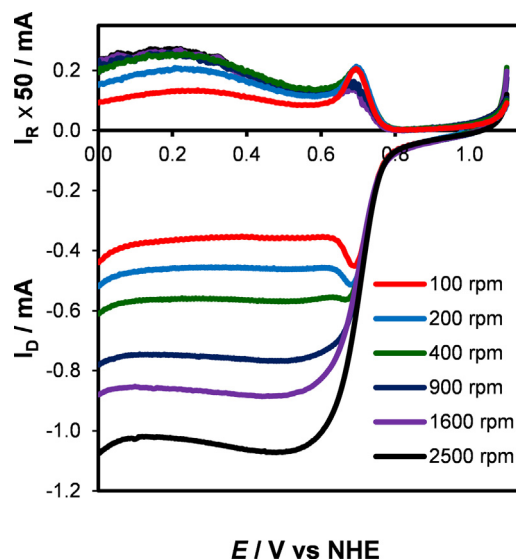


Fig. 8. Steady-state polarization curves at different rotation rates in O₂-saturated 0.5 M H₂SO₄, for ORR on Co(phen) meso 700 °C supported on Au disk (lower), and Pt ring (upper) held at 1.4 V (vs. NHE). Sweep rate: 5 mV s⁻¹; 25 °C.

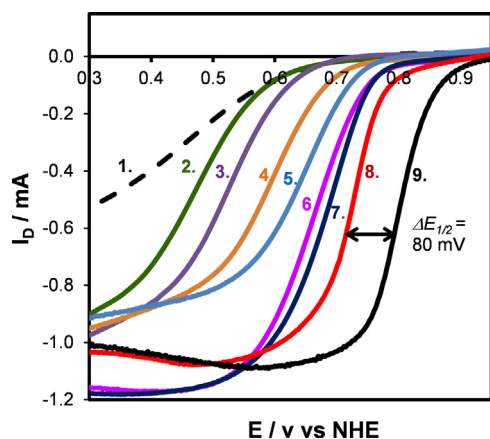


Fig. 9. Current–potential curves for ORR on selected catalysts obtained in an O₂-saturated 0.5 M H₂SO₄ solution on Au disk at 2500 rpm and 25 °C. The catalysts were obtained at 700 °C and supported on Vulcan carbon, otherwise stated. 1. Vulcan, 2. CoCl₂ Vulcan, 3. Co(ATZC), 4. Co(bis-Me-Im), 5. Co(CO₂Pz), 6. FeCo(TPTZ), 7. Co(phen), 8. Co(phen) x2 on Mesoporous carbon (higher complex load), 9. Pt 10% on Vulcan (not pyrolyzed).

with the highest N contents, as observed by XPS. Although the DPTZ ligand holds a central six membered ring with four N-heteroatoms and two pyridyl substituents, catalysts derived from it, displayed poor ORR activities at 500 °C, 700 °C and 900 °C (not shown). These results may be a consequence of the instability of the DPTZ ligand towards N=N bond cleavage and ring opening [52,53].

Five membered rings used as ligands in the precursor complexes afforded catalysts with poor ORR activity (Co(bis-Me-Im), Co(ATZC), (and Co(N-Me-Im)), what can be recognized from the higher Tafel slope (130 – 170 mV dec⁻¹, Table 2), lower number of exchanged electrons (n_e ca 3, Fig. 10), higher H₂O₂ yield (30–45 %, Fig. 11), and the lower half wave potential ($E_{1/2}$) in the voltammograms as shown in Fig. 9. These catalysts showed low ligand retention during pyrolysis (TGA) (see Fig. 3), hence a poorer N surface content was attained (XPS) (see Table 1). These catalysts showed also comparable amounts of CoO and Co metal by XRD.

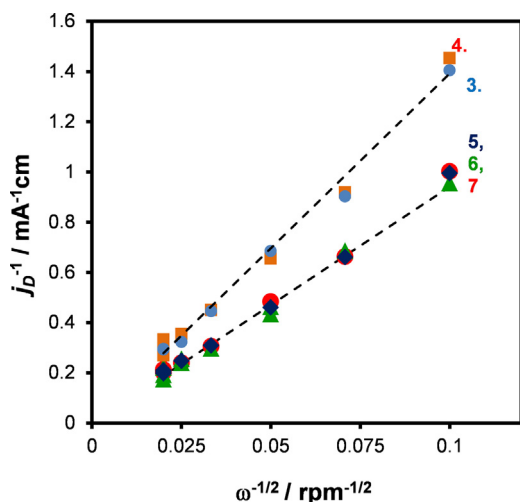


Fig. 10. Koutecky-Levich plot showing the linear relation between j_p^{-1} and $\omega^{-1/2}$ for the ORR on selected catalysts supported on Vulcan carbon and obtained at 700 °C: 3. Co(ATZC), 4. Co(bis-MeIm) (dotted line corresponding to $n_e = 2.7$), 5. Co(CO₂Pz), 6. FeCo(TPTZ), 7. Co(phen) (dotted line corresponding to $n_e = 4.0$), measured on Au disk in O₂-saturated 0.5 M H₂SO₄ solution, at 0.4 V (vs NHE). (1. Vulcan and, 2. CoCl₂ not shown).

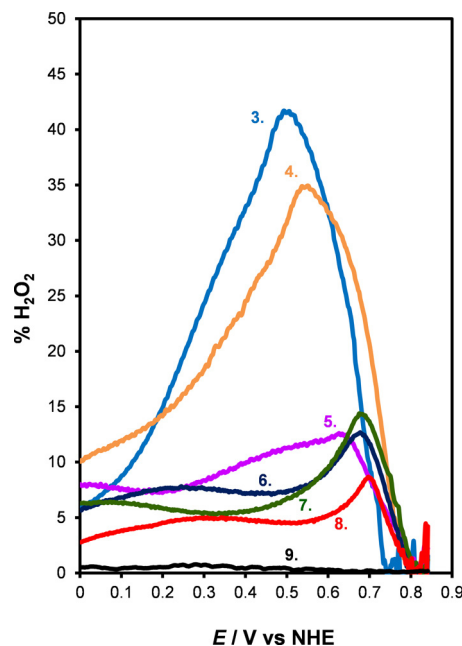


Fig. 11. Percentage of H₂O₂ produced as function of the disk potential at 100 rpm disk rotation rate (25 °C) for the ORR on selected catalysts supported on Vulcan carbon in O₂-saturated 0.5 M H₂SO₄ solution. 3. Co(ATZC), 4. Co(bis-MeIm), 5. Co(CO₂Pz), 6. FeCo(TPTZ), 7. Co(phen), 8. Co(phen) x 2 (higher complex load), 9. Pt 20% (1. Vulcan and, 2. CoCl₂ not shown). 3. – 8. pyrolyzed at 700 °C.

In all the experiments summarized in Table 2, equilibrium potential values (E_{eq}) seem to be around 0.90 ± 0.02 V, without showing any significant trend, appreciably lower than Pt catalysts whose E_{eq} lies close to 1.0 V.

The exchange current densities (j_o) range 2 – 30 $\mu\text{A cm}^{-2}$, depending mainly on the ligand, the thermal treatment and the initial complex load. Observed j_o values are comparable to those of Pt 10% on Vulcan but significantly lower than Pt 20% on the same support, which j_o resulted equal to 60 $\mu\text{A cm}^{-2}$. The Co particles were found to be ca 200 nm average diameter. This number is about one order of magnitude larger than the typical Pt particle size in commercial catalysts (ca. 3 nm). If the active sites were located on the Co metallic particles, the electrochemical active surface area (EASA) would be much smaller than that of Pt. However, observed j_o values are comparable, thus the j_o per EASA should be about one order of magnitude larger than that of Pt, hence the active sites cannot be located on the Co metallic particles.

It has been claimed that Fe catalyst show remarkable low H₂O₂ yields [25,28]. Although we found values lower than 10 % for Fe(phen) Vulcan 700 °C and Fe(CO₂Pz) Vulcan 700 °C (last not shown), the half wave potentials and Tafel parameters (see Table 2) are worse than the Co analogs. This seems to be in contradiction with some literature reports, where Fe catalysts are claimed to be superior [25,28]. Fe and Co bimetallic catalysts did not show significant improvement when compared with Co ones. Differences in ORR activities for different metals could be ascribed to different complex stabilities, N retentions, and different N speciations on the catalyst surfaces. Particularly, we found that the weight loss for Fe(phen) on Vulcan is higher than that of Co(phen) on the same substrate (data not shown).

When the initial complex load was duplicated (X2) in the Co(phen) Vulcan 700 °C catalyst, practically no changes in the electrokinetic parameters were observed, except a decrease in the H₂O₂ yield (Table 2 and Fig. SI 4). The N content did not change appreciably either (Table 1). These results may be due to surface saturation of the Vulcan support. When the Co(phen) precursor

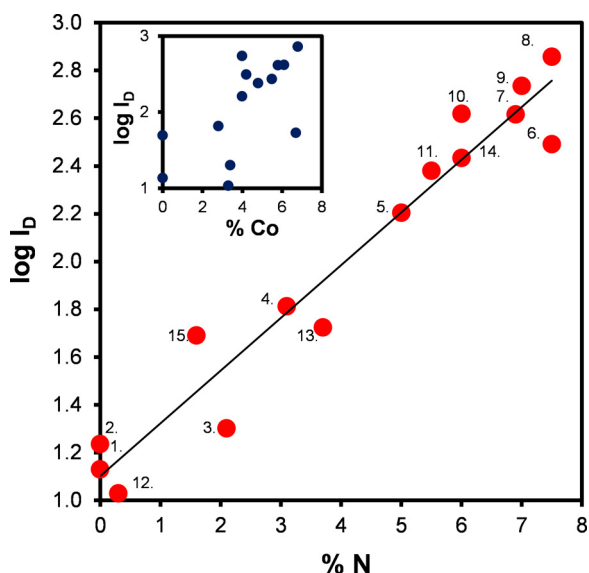


Fig. 12. Plot of the Logarithm of the disk intensity (μA , at 0.7 V vs Ag/AgCl, O_2 saturated 0.5 M H_2SO_4) vs nitrogen content (% w/w, from XPS). 1. Vulcan, 2. CoCl_2 Vulcan 700 °C, 3. Co(ATZC) Vulcan 700 °C, 4. Co(bis-Me-Im) Vulcan 700 °C, 5. $\text{Co(CO}_2\text{Pz)}$ Vulcan 700 °C, 6. FeCo(TPTZ) Vulcan 700 °C, 7. Co(phen) Vulcan 700 °C, 8. Co(phen) x2 meso 700 °C (higher complex load), 9. Co(phen) meso 700 °C, 10. $\text{Co(phen) x2 Vulcan}$ 700 °C (higher complex load), 11. Co(phen) meso 900 °C, 12. Co(phen) Vulcan 900 °C, 13. Co(phen) Vulcan 500 °C, 14. $\text{Co(phen) x2 Vulcan}$ 700 °C 0.5 M H_2SO_4 leached (8 h, 100 °C), 15. Phenanthroline Vulcan 700 °C. Inset: analogous plot for the Co content (% w/w, from XPS).

was adsorbed on a hierarchical carbon material with micro- and meso-pores and higher surface area than Vulcan carbon, ($472\text{ m}^2\text{g}^{-1}$ and $250\text{ m}^2\text{g}^{-1}$ respectively) [32], a mild shift of the polarization curve towards more positive potentials could be observed. This shift is more evident when the complex load was duplicated, exploiting the higher adsorption capacity of the mesoporous support (See Table 2 and Fig. 9). Table 1 shows that catalysts supported on the mesoporous carbon hold similar Co content (EDX), but an increased N surface concentration (XPS) when compared to Vulcan supported catalysts.

3.2.2. Cell test

The best prepared catalysts, i.e. Co(phen) meso 700 °C, Co(phen) Vulcan 700 °C, and $\text{Co(CO}_2\text{Pz)}$ Vulcan 700 °C, were used to prepare a cathode layer in a fuel cell. Polarization measurements were obtained at 90 °C using H_2 as anode fuel and O_2 at the cathode, both humidified at a flow of 150 sccm. These measurements will be improved in the near future and are shown in Fig. SI 16. The three catalysts showed a large voltage drop from the open circuit voltage (OCV) in the low current region, i.e. the activation overpotential region. This observation correlates with the lower values obtained for j_0 in comparison with a typical polarization for a Pt supported catalyst. Moreover, the order of the three catalyst evaluated correlates with the j_0 obtained: $\text{Co(phen) meso} > \text{Co(phen) Vulcan} > \text{Co(CO}_2\text{Pz)}$ Vulcan. Besides the large voltage drop, the catalyst Co(phen) meso 700 °C yielded a limiting current of 3.2 A (640 mAcm^{-2}) and a peak power of 70 mW cm^{-2} .

3.2.3. Activity-composition correlation

Fig. 12 shows a correlation between the logarithm of the intensity (measured on disk, at 0.7 V vs NHE, for the ORR reaction) vs the total nitrogen content (%N w/w) measured by XPS. A linear distribution can be observed ($R^2 = 0.94$). In the same figure, the inset corresponds to the analogous plot for the metal content (XPS), whose data are much more dispersed. Results corresponding to different precursor ligands, complex loads, carbon supports

or thermal treatments were included in Fig. 12. This correlation strongly supports the model that considers N atoms as the active sites. As stated before, ligands which are most retained during the thermal treatment (phen, TPTZ) exhibit the highest N content and also the highest ORR activity. The results presented would indicate that the mesoporous carbon provides additional area for complex adsorption and nitrogen retention during pyrolysis.

4. Conclusions

The influence of the nature of the nitrogenated ligand in the precursor complex on the catalytic activity for the oxygen reduction reaction was investigated. The synthesized catalysts were characterized by several electrochemical as well as physical bulk and surface techniques, namely XRD, TGA, Raman spectroscopy, XPS, EDX and electron microscopy. Correlating all this information, the precursor ligands can be gathered into two main groups which coincide with the number of atoms in the corresponding heterocycle ring. Catalysts prepared using five membered rings (ATZC, bis-MeIm and N-MeIm) show poorer electrokinetic parameters, higher H_2O_2 yield, lower number of exchanged electrons. These catalysts also show important amounts of Co oxides as observed by XRD. The other group is composed by the six membered ring ligands (CO_2Pz , phen and TPTZ), which show much better electrokinetic parameters, lower H_2O_2 and number of exchanged electrons close to the ideal value of 4. Phenanthroline and TPTZ were the most retained studied ligand during thermal treatment, as observed by TGA. Catalysts derived from these last ligands showed low Co oxide amounts and the highest nitrogen content (XRD and XPS respectively). Probably, formation of oxides is consequence of lower stability of the precursor complexes, which decompose during the early stages of the thermal treatment. On the other hand, the best catalysts were derived from soluble complexes (phenanthroline and TPTZ). Precipitate formation may prevent adsorption or interaction of the complexes with the carbon matrix, with the consequent lower nitrogen retention during pyrolysis.

Three different types of active sites have been proposed to be responsible of the catalytic activity of the Co-N/C catalysts, i.e. $\text{Co}^{2+}/\text{Co}^{3+}$ -N₄ active sites, Co metallic particles, and N-atoms forming part of the carbonaceous matrix (metal free catalysts). The correlation found between ORR activity and total N content strongly supports N atoms as active sites for the ORR reaction. Since all the studied samples show similar pyridinic-pyrrolic ratio (Fig. 5), analyzing the N speciation does not provide additional information on the nature of the active site. However, all the samples showed a higher proportion of pyridinic N, hence, we believe that these atoms are responsible for the ORR reaction, in agreement with previous reports [19–24].

Employing a different carbon support with a higher surface area, an appreciable improvement could be already observed in the linear sweep voltammetry and the electrokinetic parameters. This was translated in a higher power and current densities in the cell test. XPS studies showed that this catalyst held an appreciable higher N content. In this line, ligand immobilization or N-rich polymers as ligands are attractive strategies to increase the N content in the catalysts and have already been successful to improve the ORR activity.

Acknowledgements

This project was supported by the Alexander von Humboldt foundation through a Return Fellowship for FR. The authors thank financial support from the Agencia Nacional de Promoción Científica y Tecnológica (project PICT-2013-2033), the Commission

for Atomic Energy of Argentina (CNEA), and the Research Council of Argentina (CONICET). FR, FAV and MMB are researchers of CONICET. The authors acknowledge Ignacio N. Cortes (DRyT-Gerencia de Materiales-GAEN-CNEA) for measuring the XPS spectra, Cecilia A. Albornoz for the TGA measurements, Daniel R. Vega and Alicia Petragalli for obtaining the XRD patterns.

Appendix A. Supplementary data

Supplementary data associated with this article can be found, in the online version, at <http://dx.doi.org/10.1016/j.electacta.2015.05.136>.

Supplementary information: Current-potential curves at different rotation rates, Koutecky-Levich plots, H₂O₂ yield as a function of the disk potential at different rotation rates for the prepared catalysts. Complete X-Ray diffractograms, wide scan XPS spectra for some selected catalysts. This material is available free of charge via the Internet.

References

- [1] R.F. Service, Hydrogen Cars: Fad or the Future? *Science* 324 (2009) 1257.
- [2] L. Schlappbach, Technology: Hydrogen-fuelled vehicles, *Nature* 460 (2009) 809.
- [3] J. Tollefson, Hydrogen vehicles: Fuel of the future? *Nature* 464 (2010) 1262.
- [4] G. Hoogers, *Fuel Cell Technology Handbook*, CRC Press, Boca Raton, 2003.
- [5] R. Wilkinson, Fergus, X. Li, *Proton Exchange Membrane Fuel Cells: Materials Properties and Performance*, CRC, Press, Boca Raton, 2010.
- [6] H.A. Gasteiger, S.S. Kocha, B. Sompalli, F.T. Wagner, Activity benchmarks and requirements for Pt Pt-alloy, and non-Pt oxygen reduction catalysts for PEMFCs, *App. Cat. B* 56 (2005) 9.
- [7] F.T. Wagner, B. Lakshmanan, M.F. Mathias, Electrochemistry and the Future of the Automobile, *J. Phys. Chem. Lett.* 1 (2010) 2204.
- [8] R. Bashyam, P. Zelenay, A class of non-precious metal composite catalysts for fuel cells, *Nature* 443 (2006) 63.
- [9] S. Alayoglu, A.U. Nilekar, M. Mavrikakis, B. Eichhorn, Ru-Pt core-shell nanoparticles for preferential oxidation of carbon monoxide in hydrogen, *Nat. Mater.* 7 (2008) 333.
- [10] X. Zhang, L.P. Filho, C. Torres, R. Garcia-Valls, Experimental and computational study of proton and methanol permeabilities through composite membranes, *J. Power Sources* 145 (2005) 223.
- [11] J. Masa, K. Ozoemena, W. Schuhmann, J.H. Zagal, Oxygen reduction reaction using N4-metallomacrocyclic catalysts: fundamentals on rational catalyst design, *J. Porphyrins & Phthalocyanines* 16 (2012) 761–784.
- [12] C.W.B. Bezerra, L. Zhang, K. Lee, H. Liu, A.L.B. Marques, E.P. Marques, H. Wang, J. Zhang, A review of Fe–N/C and Co–N/C catalysts for the oxygen reduction reaction, *Electrochim. Acta* 53 (2008) 4937.
- [13] A. Morozan, B. Josselin, S. Palacin, Low-platinum and platinum-free catalysts for the oxygen reduction reaction at fuel cell cathodes, *Energy & Environmental Sci.* 4 (2011) 1238.
- [14] R. Jasinski, A New Fuel Cell Cathode Catalyst, *Nature* 201 (1964) 1212.
- [15] M. Jahnke, H. Schonborn, G. Schonborn, M. Zimmermann, G. Zimmermann, Organic dyestuffs as catalysts for fuel cells, *Top. Curr. Chem.* 61 (1976) 133.
- [16] J.-P. Dodelet, Oxygen Reduction in PEM Fuel Cell Conditions: Heat-Treated Non-Precious Metal-N4 Macrocycles and Beyond, in: F.B.J.H. Zagal, J.P. Dodelet (Eds.), *N4-Macrocyclic Metal Complexes*, Springer-Verlag, New York, 2006, pp. 83.
- [17] A.B.A. Garsuch, G. Liu, R. Yang, J.R. Dahn, Time to move beyond transition metal–N–C catalysts for oxygen reduction, in: A.L.W. Vielstich, H.A. Gasteiger (Eds.), *Handbook of Fuel Cells – Fundamentals, Technology and Applications*, Wiley, Chichester, UK, 2009, pp. 71.
- [18] P.P.C.M. Johnston, P. Zelenay, Transition metal/polymer catalysts for O₂ reduction, in: A.L.W. Vielstich, H.A. Gasteiger (Eds.), *Handbook of Fuel Cells – Fundamentals, Technology and Applications*, Wiley, Chichester, UK, 2009, pp. 48.
- [19] X. Zhou, J. Qiao, L. Yang, J. Zhang, A Review of Graphene-Based Nanostructural Materials for Both Catalyst Supports and Metal-Free Catalysts in PEM Fuel Cell Oxygen Reduction Reactions, *Adv. Energy Mat.* 4 (2014) 1301523.
- [20] W. He, C. Jiang, J. Wang, L. Lu, High-Rate Oxygen Electroreduction over Graphitic-N Species Exposed on 3D Hierarchically Porous Nitrogen-Doped Carbons, *Angew. Chem. Int. Ed.* 53 (2014) 9503.
- [21] Y. Jiao, Y. Zheng, M. Jaroniec, S.Z. Qiao, Origin of the Electrocatalytic Oxygen Reduction Activity of Graphene-Based Catalysts: A Roadmap to Achieve the Best Performance, *J. Am. Chem. Soc.* 136 (2014) 4394.
- [22] J.P. Dodelet, The Controversial Role of the Metal in Fe- or Co-Based Electrocatalysts for the Oxygen Reduction Reaction in Acid Medium, in: S. Minhua (Ed.), *Electrocatalysis in Fuel Cells*, Lecture Notes in Energy, Springer, London, 2013, pp. 271.
- [23] C.E. Szakacs, M. Lefevre, U.I. Kramm, J.-P. Dodelet, F. Vidal, A density functional theory study of catalytic sites for oxygen reduction in Fe/N/C catalysts used in H₂/O₂ fuel cells, *Phys. Chem. Chem. Phys.* 16 (2014) 13654.
- [24] U.I. Kramm, J. Herranz, N. Larouche, T.M. Arruda, M. Lefevre, F. Jaouen, P. Bogdanoff, S. Fiechter, I. Abs-Wurmbach, S. Mukerjee, J.-P. Dodelet, Structure of the catalytic sites in Fe/N/C-catalysts for O₂-reduction in PEM fuel cells, *Phys. Chem. Chem. Phys.* 14 (2012) 11673.
- [25] G. Wu, K.L. More, C.M. Johnston, P. Zelenay, High-Performance Electrocatalysts for Oxygen Reduction Derived from Polyaniline, Iron, and Cobalt, *Science* 332 (2011) 443.
- [26] T. Onodera, S. Suzuki, T. Mizukami, H. Kanzaki, Enhancement of oxygen reduction activity with addition of carbon support for non-precious metal nitrogen doped carbon catalyst, *J. Power Sources* 196 (2011) 7994.
- [27] R. Silva, D. Voiry, M. Chhowalla, T. Asefa, Efficient Metal-Free Electrocatalysts for Oxygen Reduction: Polyaniline-Derived N- and O-Doped Mesoporous Carbons, *J. Am. Chem. Soc.* 135 (2013) 7823.
- [28] S. Ganesan, N. Leonard, S.C. Barton, Impact of transition metal on nitrogen retention and activity of iron-nitrogen-carbon oxygen reduction catalysts, *Phys. Chem. Chem. Phys.* 16 (2014) 4576.
- [29] J. Tian, A. Morozan, M.T. Sougrati, M. Lefevre, R. Chenitz, J.-P. Dodelet, D. Jones, F. Jaouen, Optimized Synthesis of Fe/N/C Cathode Catalysts for PEM Fuel Cells: A Matter of Iron-Ligand Coordination Strength, *Angew. Chem. Int. Ed.* 52 (2013) 6867.
- [30] J.-S. Li, S.-L. Li, Y.-J. Tang, K. Li, L. Zhou, N. Kong, Y.-Q. Lan, J.-C. Bao, Z.-H. Dai, Heteroatoms ternary-doped porous carbons derived from MOFs as metal-free electrocatalysts for oxygen reduction reaction, *Scientific Reports* 4 (2014) 5130.
- [31] Y. Ren, G.H. Chia, Z. Gao, Metal-organic frameworks in fuel cell technologies, *Nano Today* 8 (2013) 577.
- [32] M.M. Bruno, H.R. Corti, J. Balach, N.G. Cotella, C.A. Barbero, Hierarchical porous materials: capillaries in nanoporous carbon, *Functional Mat. Lett.* 02 (2009) 135.
- [33] S. Li, L. Zhang, J. Kim, M. Pan, Z. Shi, J. Zhang, Synthesis of carbon-supported binary FeCo–N non-noble metal electrocatalysts for the oxygen reduction reaction, *Electrochim. Acta* 55 (2010) 7346.
- [34] D.M.L. Goodgame, M. Goodgame, G.W. Rayner-Canham, Spectroscopic studies of substituted imidazole complexes. II. N-methylimidazole complexes of divalent cobalt, nickel, copper and zinc, *Inorg. Chimica Acta* 3 (1969) 406.
- [35] Y.-C. Liang, M.-C. Hong, J.-C. Liu, R. Cao, Hydrothermal syntheses, structural characterizations and magnetic properties of cobalt(II) and manganese(II) coordination polymeric complexes containing pyrazinecarboxylate ligand, *Inorg. Chimica Acta* 328 (2002) 152.
- [36] S. De Angelis Curtis, K. Kurdziel, S. Materazzi, S. Vecchio, Crystal structure and thermoanalytical study of cobalt(II) and nickel(II) complexes with 2,2'-bis-(4,5-dimethylimidazole), *Thermochimica Acta* 510 (2010) 75.
- [37] F.A. Westerhaus, R.V. Jagadeesh, G. Wienhöfer, M.-M. Pohl, J. Radnik, A.-E. Surkus, J. Rabeah, K. Junge, H. Junge, M. Nielsen, A. Brückner, M. Beller, Heterogenized cobalt oxide catalysts for nitroarene reduction by pyrolysis of molecularly defined complexes, *Nat. Chem.* 5 (2013) 537.
- [38] H. Collins, Smith, 2,4,6-Tripyridyl-s-triazine as Reagent for Iron. Determination of Iron in Limestone, Silicates, and Refractories, *Analytical Chem.* 31 (1959) 1862.
- [39] T.S. Lee, I.M. Kolthoff, D.L. Leussing, Reaction of Ferrous and Ferric Iron with 1,10-Phenanthroline. I. Dissociation Constants of Ferrous and Ferric Phenanthroline, *J. Am. Chem. Soc.* 70 (1948) 2348.
- [40] B.J. Tufts, I.L. Abrahams, C.E. Caley, S.R. Lunt, G.M. Miskelly, M.J. Sailor, P.G. Santangelo, N.S. Lewis, A.L. Roe, K.O. Hodgson, XPS and EXAFS studies of the reactions of cobalt(III) ammine complexes with gallium arsenide surfaces, *J. Am. Chem. Soc.* 112 (1990) 5123.
- [41] X. Chen, H. Ren, W. Peng, H. Zhang, J. Lu, L. Zhuang, Highly Efficient Molecular Cobalt Electrode for (Photo) electrochemical Hydrogen Evolution, *J. Phys. Chem. C* 118 (2014) 20791.
- [42] E.A. Franceschini, M.M. Bruno, F.A. Viva, F.J. Williams, M. Jobbágy, H.R. Corti, Mesoporous Pt electrocatalyst for methanol tolerant cathodes of DMFC, *Electrochim. Acta* 71 (2012) 173.
- [43] H.-D. Sha, X. Yuan, X.-X. Hu, H. Lin, W. Wen, Z.-F. Ma, Effects of Pyrrole Polymerizing Oxidant on the Properties of Pyrolysed Carbon-Supported Cobalt-Polypyrrole as Electrocatalysts for Oxygen Reduction Reaction, *J. Electrochem. Soc.* 160 (2013) F507.
- [44] K. Artyushkova, S. Levendosky, P. Atanassov, J. Fulghum, XPS Structural Studies of Nano-composite Non-platinum Electrocatalysts for Polymer Electrolyte Fuel Cells, *Top. Catal.* 46 (2007) 263.
- [45] N.A.M. Barakat, B. Kim, S.J. Park, Y. Jo, M.-H. Jung, H.Y. Kim, Cobalt nanofibers encapsulated in a graphite shell by an electrospinning process, *J. Mat. Chem.* 19 (2009) 7371.
- [46] H.C. Choi, Y.M. Jung, I. Noda, S.B. Kim, A Study of the Mechanism of the Electrochemical Reaction of Lithium with CoO by Two-Dimensional Soft X-ray Absorption Spectroscopy (2D XAS), 2D Raman, and 2D Heterospectral XAS-Raman Correlation Analysis, *J. Phys. Chem. B* 107 (2003) 5806.
- [47] K. Niu, B. Yang, J. Cui, J. Jin, X. Fu, Q. Zhao, J. Zhang, Graphene-based non-noble-metal Co/N/C catalyst for oxygen reduction reaction in alkaline solution, *J. Power Sources* 243 (2013) 65.
- [48] N. Mahmood, C. Zhang, H. Yin, Y. Hou, Graphene-based nanocomposites for energy storage and conversion in lithium batteries, supercapacitors and fuel cells, *J. Mat. Chem. A* 2 (2014) 15.
- [49] H.-J. Zhang, H. Li, X. Li, H. Qiu, X. Yuan, B. Zhao, Z.-F. Ma, J. Yang, Pyrolyzing cobalt diethylenetriamine chelate on carbon (CoDETA/C) as a family of non-

- precious metal oxygen reduction catalyst, *Int. J. Hydrogen Energy* 39 (2014) 267.
- [50] N.P. Subramanian, S.P. Kumaraguru, H. Colon-Mercado, H. Kim, B.N. Popov, T. Black, D.A. Chen, Studies on Co-based catalysts supported on modified carbon substrates for PEMFC cathodes, *J. Power Sources* 157 (2006) 56.
- [51] J. Qiao, L. Xu, L. Ding, L. Zhang, R. Baker, X. Dai, J. Zhang, Using pyridine as nitrogen-rich precursor to synthesize Co-N-S/C non-noble metal electrocatalysts for oxygen reduction reaction, *App. Cat. B* 125 (2012) 197.
- [52] J. Cui, L. Huang, Z. Lu, Y. Li, Z. Guo, H. Zheng, Synthesis and properties of five unexpected copper complexes with ring-cleavage of 3,6-di-2-pyridyl-1,2,4,5-tetrazine by one pot in situ hydrothermal reaction, *Cryst. Eng. Comm.* 14 (2012) 2258.
- [53] P. Yang, S. Chen, Y. Liu, Z. Xiao, L. Ding, A pyridine-functionalized pyrazolinofullerene used as a buffer layer in polymer solar cells, *Phys. Chem. Chem. Phys.* 15 (2013) 17076.